Hindawi
Wireless Communications and Mobile Computing
Volume 2022, Article ID 7399457, 14 pages
https://doi.org/10.1155/2022/7399457

Research Article

Highly Efficient MIMO-OFDM with Index Modulation

Zeng Hu,[1] **Dehuan Wan**,[2] **Yankun Chen**,[3] **Jinpei Yan**,[4] **Yun Liu**,[2] **Pengfei Guo**,[5] **Liming Chen**,[6] **and Wen Zhou**[7]

[1]*College of Information Science and Technology, Zhongkai University of Agriculture and Engineering, Guangzhou 510225, China*
[2]*Center for Data Science and Artificial Intelligence, Guangdong University of Finance, Guangzhou 510521, China*
[3]*South China Sea Marine Survey and Technology Center, State Oceanic Administration, Guangzhou 510300, China*
[4]*School of Computer Science and Engineering, Xi'an University of Technology, Xi'an 710048, China*
[5]*School of Computational Science, Zhongkai University of Agriculture and Engineering, Guangzhou 510225, China*
[6]*Electric Power Research Institute of CSG, Guangzhou 510663, China*
[7]*School of Information Engineering, Nanjing Forestry University, Nanjing 210037, China*

Correspondence should be addressed to Dehuan Wan; wan_e@gduf.edu.cn

Received 9 May 2022; Accepted 29 June 2022; Published 22 July 2022

Academic Editor: Yingyang Chen

Index modulation (IM) is a novel digital modulation technique, which inactivates some subcarriers in orthogonal frequency division multiplexing (OFDM) to exploit the indices of the subcarriers to transmit bits implicitly, and has potential to further improve the energy efficiency and error performance. For the multiple-input multiple-output- (MIMO-) aided IoT devices, a highly efficient and low-complexity IM-aided scheme is needed to reduce the computational complexity at the receiver sides. In this paper, we propose a novel highly efficient MIMO-OFDM with IM scheme by performing IM on each transmit antenna subgroup, which contains two transmit antennas, to achieve two transmit diversity order and significant reduction in computational complexity at the cost of a minor spectral efficiency. To reduce the demodulation complexity, a low-complexity sequential Monte Carlo (SMC) theory-based detector is proposed, which exploits the null space submatrix of the preprocessed channel response matrix by using QR decomposition, to calculate the most likely transmitted IM patterns before the detection of the modulated symbols. Computer simulation results and complexity analysis show that the proposed IM-aided scheme achieves better error performance with extremely low computational complexity under the same constellation and the proposed SMC detector has potential to achieve near optimal bit error rate performance with considerably low demodulation complexity.

1. Introduction

The next-generation wireless communication networks will enable various types of devices with different requirements in enhanced mobile broadband (eMBB), massive machine type of communication (mMTC), and ultrareliable and low-latency communication (uRLLC) scenarios [1, 2]. In beyond fifth-generation (B5G) wireless communication networks and the sixth-generation (6G) wireless communication networks, the ubiquitous infrastructure devices and various Internet of Things (IoT) in industry, home, hospital, smart agriculture, and other scenarios will dominate the terminal side in the next decade [3–5]. As a typical smart devices in mMTC scenario, IoT in most applications are known for its low cost, battery dependent, low power consumption, and limited computing capability equipment, which put forward higher requirements in data transmission and computational complexity. To support machine type of communication (MTC), narrow band IoT (NB-IoT) is specified as the long-term evolution for machine-type (LTE-M) communication by the third-generation partnership project (3GPP) in the fourth-generation (4G) LTE. For the energy and computing capability sensitive devices, low power consumption wireless communication techniques and low-complexity transceiver algorithms are crucial for prolonging the

lifetime and enhancing the robustness of the mMTC networks [6–8].

Index modulation (IM) is a novel emerged promising technique which exploits the index domain of some building blocks of a communication system, such as antennas, time slots, frequency subcarriers, multiple symbol mode or constellation, and signal processing matrices, to convey information bits to meet the demands of low energy consumption and high data transmission [9–12]. To alleviate the interantenna synchronization (IAS) problem at the transmitter and reduce the signal processing complexity at the receiver, spatial modulation (SM), which exploits the index domain of the transmit antennas in a multiple-input multiple-output (MIMO) system, has been proposed to activate one antenna according to the input information bits to transmit the modulated symbol [12–14]. It is clearly that there are two ways to transmit the information bits in SM, which are known as the conventional modulated symbols and the index patterns of the transmit antennas. For the clarity of presentation, we define the information bits transmitted by the modulated symbols and the index patterns are modulation bits and index bits, respectively. To further increase the spectral efficiency (SE), a subgroup of transmit antennas are activated to transmit modulated symbols in generalized SM (GSM) [15, 16]. Then, a novel dual-hop SM-aided relay network is proposed to transmit its own information while forwarding the SM signal to the destination with both decode-and-forward and amplify-and-forward protocols [17]. To reduce the computational complexity in soft decision, the deterministic sequential Monte Carlo- (SMC-) based detectors are proposed for single-carrier (SC) GSM [18]. In [19], the K-best sphere decoding (SD) soft detection algorithm is proposed to effectively detect the active antennas and the modulated symbols by exploiting the null space of the GSM channel based on the QL decomposition.

In 4G, 5G, and wireless local area network (WLAN) communication standards, orthogonal frequency division multiplexing (OFDM) has become one of the most dominant multicarrier techniques due to its merits in combating with the frequency selective Rayleigh fading channel [20–23]. Owing to the superior of bit error rate (BER) performance and flexible design introduced by the IM technique, IM-aided schemes have attracted considerable attention over the past few years. By applying IM in the frequency subcarrier domain, OFDM with index modulation (OFDM-IM), which appears as a competitive candidate alternative to conventional OFDM, exhibits better bit error rate performance and higher energy efficiency than those of conventional OFDM [24–27]. In this paper, let us define the subcarrier activation patterns (SAPs) to denote the IM patterns of the active statues of the subcarriers within one subblock after the signal processing of the IM. The achievable rate and mutual information of OFDM-IM are analyzed, which shows that OFDM-IM has potential to outperform conventional OFDM [28, 29]. An intercarrier interference (ICI) self-cancellation scheme is proposed to alleviate the effect in the presence of ICI in the underwater acoustic communication scenario [30]. Then, a novel enhanced coordinate interleaving OFDM-IM is proposed to improve the BER performance of the index bits [31]. By introducing IM in the spread spectrum, a novel index-modulated OFDM spread spectrum is proposed to exploit the index domain of spreading codes [32]. Then, an IM-aided subcarrier mapping scheme is proposed for dual-hop OFDM-based relay networks with different relay protocols [33] and an OFDM-IM-based distributed cooperative system is analyzed in [34]. To further improve the SE, a dual mode scheme is proposed in which another distinguishable constellation is transmitted at the inactive subcarriers [35]. Moreover, by dividing the constellation into several distinguishable subconstellations, multiple mode- (MM-) aided OFDM-IM scheme is proposed to further improve the system SE and the BER performance [36–38]. By utilizing silent subcarriers and MM, a transmit diversity scheme for OFDM-IM is proposed to further improve the system error performance [39]. In [40], a novel cascade IM scheme is proposed by performing MM IM onto the activated subcarriers in OFDM-IM, which combines the advantages of both MM IM and conventional OFDM-IM and can further enhance the system error performance.

In OFDM-IM, the available subcarriers in each block are divided into several subblocks to reduce the modulation and demodulation complexity. The dependence of the active statuses of the subcarriers in each subblock make the demodulation of the optimal maximum likelihood (ML) detector should be performed in subblock-wise, which leads to extremely high computational complexity at the receiver side. By taking the advantage of the orthogonality of the subcarriers in OFDM, a subcarrier-wise ML detector, which calculates the most likely transmitted symbols in subcarrier-wise using the ML criterion and makes the decision of the estimate of the transmitted symbol vector in subblock-wise, is proposed to reduce computational complexity at the receiver [41]. To further reduce the demodulation complexity, a series of low-complexity detection algorithms, which have potential to achieve near-optimal BER performance, are proposed for OFDM-IM, such as minimum mean square error (MMSE) detector [24], subcarrier-wise-based tree search detectors [41], and log-likelihood ratio- (LLR-) based detectors [42]. With the aid of the low-complexity detection algorithms, OFMD-IM has potential to achieve the same order of the detection complexity as that of conventional OFDM.

MIMO is another key technique for the next-generation wireless networks, which can improve the BER performance and the data rate of the systems [43]. To harvest the advantages of both IM and MIMO techniques, MIMO-OFDM with index modulation (MIMO-OFDM-IM) is proposed to meet the requests of high date rate and reliable data transmission in B5G and 6G [44, 45]. Owing to the advantage of IM in BER performance, MIMO-OFDM-IM exhibits ability to surpass conventional MIMO-OFDM. Specifically, MIMO-OFDM-IM achieves superior BER performance due to the robustness of the index bits, which is theoretically analyzed in [46]. Compared with conventional MIMO-OFDM, MIMO-OFDM-IM can provide an interesting trade-off between SE, error performance, and performing complexity, which provides a more flexible transceiver design.

In MIMO-OFDM-IM, each antenna transmit independent OFDM-IM block, which means that independent

OFDM-IM process is implemented in each branch. Inheriting from OFDM-IM, the dependence of the active statuses of the subcarriers within each subblock makes the detection process becomes an intricate problem. For convenience of expression, we define antenna activation patterns (AAPs) to denote the active statuses of the transmit antennas of each subcarrier level after IM in each transmit antenna. By exploiting the orthogonality of the subcarriers within each subblock, the most likely transmitted symbol vectors under the condition of different AAPs are analyzed in [47], which shows that the optimal error performance can be obtained by performing subcarrier-wise ML detection in the first step and full search of SAPs under the constrain of the IM lookup table of OFDM-IM in each transmit antenna level in the second step. Clearly, each AAP corresponds to a most likely transmitted symbol vector in the subcarrier-wise detection at the receiver. To further alleviate the computational burden at the receiver, LLR-based detectors [44], ordered successive interference cancellation-(OSIC-) based MMSE detector [46], and SMC theory-based detectors [47, 48] are proposed for the detection of MIMO-OFDM-IM. Although subcarrier-wise detection algorithms have reduced the demodulation complexity tremendously, the number of the AAPs increases exponentially with the number of the transmit antenna, which limits the applications of MIMO-OFDM-IM in the mMTC scenarios. Therefore, higher efficient IM-aided schemes and low-complexity detection algorithms are critical to the mMTC scenario.

To this end, we propose a novel highly efficient (HE-) MIMO-OFDM-IM scheme for the mMTC scenario, which has a fixed number of the activated transmit antennas at each subcarrier level, to improve the error performance and reduce the computational complexity of signal processing at both transceiver sides. In the proposed HE-MIMO-OFDM-IM scheme, the transmit antennas are divided into several subgroups, and IM is performed within each transmit antenna subgroup to achieve higher transmit diversity. With the fixed number of the activated transmit antennas for all the subcarriers at the antenna dimension, the AAPs, which are similar to those of the SM scheme, are obtained in HE-MIMO-OFDM-IM. Unlike the number of the activated transmit antennas ranges from zero to the number of the transmit antennas N_T in classical MIMO-OFDM-IM scheme, HE-MIMO-OFDM-IM can use the low-complexity detection algorithms for the SM schemes to further reduce the detection complexity of each subcarrier level, which means that the proposed scheme can achieve near same computational complexity level as SM and harvests the benefits of OFDM-IM. The main contributions of this paper are summarized as follows:

(i) A novel HE-MIMO-OFDM-IM scheme is proposed to reduce the computational complexity at both the transmitter and receiver sides. By dividing the transmit antennas into several subgroups, higher order of transmit diversity of index patterns and lower demodulation complexity at the receiver can be realized with the aid of the novel IM structure at the transmitter

(ii) A subcarrier-wise detection architecture, which exploits the AAPs in transmit antenna dimension to detect the most likely transmitted symbol vectors subcarrier by a subcarrier, is proposed for HE-MIMO-OFDM-IM to easily lift the demodulation burden at the receiver. Then, the computational complexity in terms of the floating-point operations (FLOPs) is analyzed for different detectors, which shows that the proposed HE-MIMO-OFDM-IM can provide a significant reduction in demodulation complexity compared with conventional MIMI-OFDM-IM under the same MIMO configuration

(iii) A low-complexity two-step SMC detector is proposed for HE-MIMO-OFDM-IM, which exploits the null space submatrix based on the QR decomposition of the preprocessed channel response matrix to calculate the most likely transmitted IM patterns in the first step and employs SMC theory to detect the most likely transmitted symbol vectors of each subcarrier based of the IM patterns obtained in the first step. The simulation results in term of the BER performance of HE-MIMO-OFDM-IM show that the proposed SMC detector has potential to achieve near-optimal BER performance with considerably low computational complexity

The remainder of this paper is organized as follows. The system model of HE-MIMO-OFDM-IM and the optimal ML detector are given in Section 2. Then, a low-complexity detectors is proposed in Section 3. Computer simulation results are given in Section 4. Finally, Section 5 concludes the paper.

Notation: $\mathbf{X}$ denotes a matrix and $\mathbf{x}$ denotes a column-vector. $(\cdot)^T$ and $(\cdot)^H$ denote transposition and Hermitian transposition of a matrix or a vector, respectively. diag $\{\mathbf{x}\}$ returns a diagonal matrix whose diagonal elements are included in $\mathbf{x}$. $x \sim \mathcal{CN}(0, \sigma_x^2)$ represents the distribution of a zero mean circularly symmetric complex Gaussian random variable x with variance σ_x^2. $\lfloor \cdot \rfloor$ is the integer floor operation, and $\varnothing$ denotes the empty set. $\|\cdot\|$ stands for Frobenius norm. $|\cdot|$ denotes the absolute value of a complex number. $C(\cdot, \cdot)$ denotes the binomial coefficient. $p(\cdot)$ denotes the probability of an event. $\mathcal{S}$ denotes the complex symbol constellation of size M. $\mathcal{O}(\cdot)$ denotes the order of detection complexity with respect to the constellation size. FFT$\{\cdot\}$ denotes the fast Fourier transform (FFT) operator, and IFFT$\{\cdot\}$ denotes the inverse FFT operator.

2. System Model

In this section, we present the transceiver structure and the signal model of HE-MIMO-OFDM-IM.

2.1. Transmitter. In this paper, we consider a wireless communication scenario in which the devices are equipped with N_T transmit antennas and N_R receive antennas. A basic block diagram of the MIMO communication model for the proposed HE-MIMO-OFDM-IM is shown in Figure 1. In HE-MIMO-OFDM-IM, the transmit antennas are divided into N_{TA} subgroups, each of which contains two antennas, where $N_{TA} = N_T/2$. In each subgroup, we can choose two

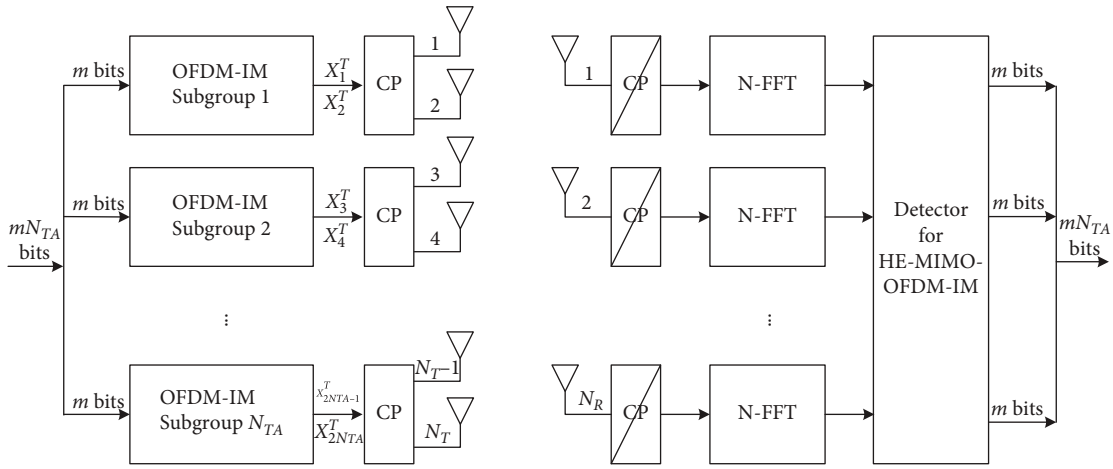

Figure 1: Transceiver structure of the HE-MIMO-OFDM-IM system.

adjacent transmit antennas or interleaved transmit antennas to form a subgroup, which are termed as localized grouping and interleaved grouping, respectively. Since modulation and demodulation for the localized grouping and interleaved grouping methods follow the identical procedures, we thereafter take two adjacent transmit antennas to form a subgroup to illustrate the signal processes of the proposed HE-MIMO-OFDM-IM.

In HE-MIMO-OFDM-IM, independent OFDM-IM process is performed within each transmit antenna subgroup. For each transmit antenna subgroup, the available N subcarriers are equally partitioned into G subblocks to perform independent IM to reduce the modulation complexity, each of which contains $N_S = N/G$ subcarriers. The basic block diagram of OFDM-IM for each transmit antenna subgroup is given in Figure 2. At each transmission block, a total number of mN_{TA} input information bits are equally separated into N_{TA} subgroups to fed into each transmit antenna subgroup, each of which contains m information bits. Then, the corresponding m input information bits are further divided into G subgroups for each subblock, each of which contains $p = m/G$ information bits. The IM processes in all the subblocks are the same and independent of each other, so let us take the gth subblock of the n_{ta}th transmit antenna subgroup as an illustrative case to show the procedures, where $g \in \{1, 2, \cdots, G\}$, $n_{ta} \in \{1, 2, \cdots, N_{TA}\}$. According to the principle of IM, K out of N_S subcarriers within the subblock are selected as the active subcarriers to transmit the modulated symbols, which indicates that there are total $C(N_S, K)$ available SAPs for the IM of each subblock. In this paper, we define $C\,N_S, K$ to denote that there are N_S subcarriers in the subblock and K subcarriers are activated to transmit modulated symbols. For each subblock, the input p information bits are transmitted by two ways, the first way is $p_1 = \log_2 \lfloor C(N_S, K) \rfloor$ index bits transmitted implicitly by the SAPs, while the second way is $p_2 = N_S \log_2 M$ modulation bits transmitted by N_S modulated symbols, where M is the order of the modulated symbol constellation.

In IM process, the index selector chooses one SAP according to the p_1 information bits based on the SAPs lookup table or the combinatorial method. Since $N_{\mathrm{SAP}} = 2^{p_1} \le C(N_S, K)$, there are always some unused SAPs in IM, which are treated as illegal SAPs and should be avoided in the subcarrier-wise detectors. For the gth subblock of the n_{ta}th transmit antenna subgroup, the output of the SAPs selector for the first antenna in the subgroup is given by

$$\mathcal{I}_i^{(n_{ta},g)} = \{n_1, n_2, \cdots, n_K\}, \tag{1}$$

where $i \in \{1, 2, \cdots, N_{\mathrm{SAP}}\}$ is the index of SAPs, $n_k \in \{1, 2, \cdots, N_S\}$, $n_j \neq n_k$ if $j \neq k$, and the elements in $\mathcal{I}^{(n_{ta},g)}$ are sorted in ascending order. The SAP of the second antenna in the n_{ta}th transmit antenna subgroup is defined as the complementary set of the $\mathcal{I}^{(n_{ta},g)}$, which can be expressed as

$$\bar{\mathcal{I}}_i^{(n_{ta},g)} = \{\bar{n}_1, \bar{n}_2, \cdots, \bar{n}_{N_S-K}\}, \tag{2}$$

where the elements in $\bar{\mathcal{I}}_i^{(n_{ta},g)}$ are sorted in ascending order, $\bar{n}_k \in \{1, 2, \cdots, N_S\}$, $\bar{n}_j \neq \bar{n}_k$ if $j \neq k$, $\mathcal{I}_i^{(n_{ta},g)} \cup \bar{\mathcal{I}}_i^{(n_{ta},g)} = \{1, 2, \cdots, N_S\}$, $\mathcal{I}_i^{(n_{ta},g)} \cap \bar{\mathcal{I}}_i^{(n_{ta},g)} = \varnothing$. Then, the $N_S \times 1$ modulated symbol vector is generated according to the rest p_2 information bits, where the output of the M-ary symbol modulator is given by

$$\mathbf{s}^{(n_{ta},g)} = \left[s_1, s_2, \cdots, s_K, s_{K+1}, \cdots s_{N_S}\right]^T, \tag{3}$$

where $s_k \in \mathcal{S}$ is an element of M-ary quadrature amplitude modulation (QAM) or phase-shift keying (PSK) constellation, $k = 1, 2, \cdots, N_S$. In $\mathbf{s}^{(n_{ta},g)}$, the first K modulated symbols are used to generate the transmitted symbol vector of the first transmit antenna, and the rest are for the second transmit antenna. We assume that the modulated symbols are normalized to unit average power, i.e. $E\{\mathbf{s}\mathbf{s}^H\} = N_S$. Then, the OFDM-IM subblock creator maps the modulated symbols to the activated subcarriers according to the obtained SAPs. The final $N_S \times 1$ transmitted symbol

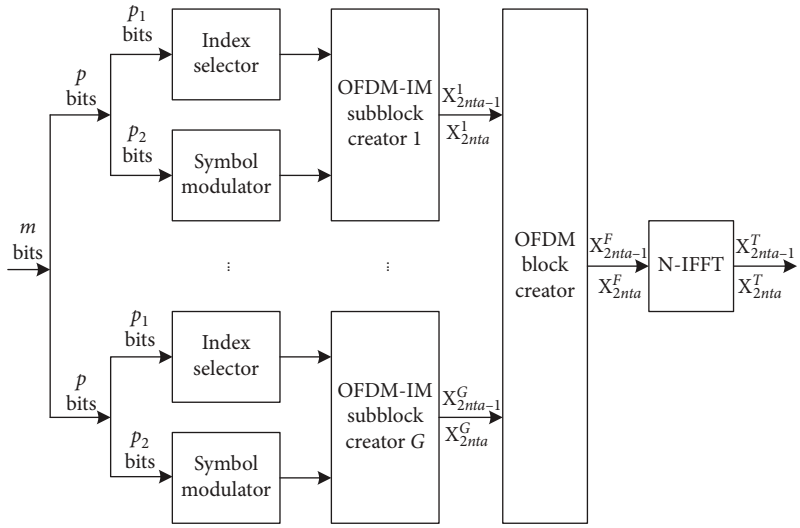

Figure 2: Block diagram of the OFMD-IM transmitter in each transmit antenna subgroup.

vector of the first transmit antenna, whose index is given by $2n_{ta}-1$, can be expressed as

$$\mathbf{x}^g_{2n_{ta}-1} = \left[x^g_1, x^g_2, \cdots, x^g_{N_S}\right]^T, \tag{4}$$

where $x^g_k \in \{\mathcal{S}, 0\}$, $k = 1, 2, \cdots, N_S$. Similarly, the $N_S \times 1$ transmitted symbol vector of the second transmit antenna with index $2n_{ta}$ is given by

$$\mathbf{x}^g_{2n_{ta}} = \left[x^g_1, x^g_2, \cdots, x^g_{N_S}\right]^T. \tag{5}$$

After G subblocks corresponding to each transmit antenna are obtained, the transmitted symbol vector can be generated by concatenating these modulated symbol vectors in order. The transmitted symbol vectors of the n_{ta}th transmit antenna subgroup are given by

$$\mathbf{x}^F_t = \left[\left(\mathbf{x}^1_t\right)^T, \left(\mathbf{x}^2_t\right)^T, \cdots, \left(\mathbf{x}^G_t\right)^T\right]^T, \tag{6}$$

where the index of transmit antenna is given by $t = 2n_{ta} - 1, 2n_{ta}$, $n_{ta} = 1, 2, \cdots, N_{TA}$. After this point, independent inverse fast Fourier transform (IFFT) for each transmit antenna is performed to generate the time domain transmitted symbol vector, which is given by

$$\mathbf{x}^T_t = \mathrm{IFFT}\left(\mathbf{x}^F_t\right) = \left[x^T_1, x^T_2, \cdots x^T_N\right]^T, \tag{7}$$

where $t = 2n_{ta} - 1, 2n_{ta}$ and $n_{ta} = 1, 2, \cdots, N_{TA}$. A cyclic prefix (CP) of N_{CP} samples, which is longer than the number of the channel taps, is appended to the beginning of the time domain transmitted symbol vector in each transmit antenna. Then, identical procedures as conventional OFDM such as parallel to serial and digital-to-analog are performed to get the high-frequency broadband signals, which are sent simultaneously from all the transmit antennas to the destination. We assume that the frequency selective Rayleigh fading channel remains constant during one block and changes blast to blast. For the clarity of presentation, an example of IM process is given as follows.

Example 1. In HE-MIMO-OFDM-IM, two transmit antennas form a subgroup as a unit for IM to maintain fixed number of the activated transmit antennas for each subcarrier. We assume the parameters in HE-MIMO-OFDM-IM are given by $N_T = N_R = 4$, $N_{TA} = 2$, $N_S = 4$, $K = 2$, and $M = 16$. Table 1 gives an example of SAP lookup table and the corresponding complementary set. Without loss of generality, we take the modulation process of the gth subblock as an illustrative case. In this case, a total of $p_1 = 2$ index bits and $p_2 = 16$ modulation bits can be transmitted per subblock. For convenience of expression, let us define $p_1^{(n_{ta})}$ to denote the index bits of the n_{ta}th transmit antenna subgroup, $n_{ta} = 1, 2, \cdots, N_{TA}$. Assuming the input index bits for two transmit antenna subgroups of the gth subblock are given by $p_1^{(1)} = [1, 0]$ and $p_1^{(2)} = [0, 0]$. The SAP and the complementary set of the first transmit antenna subgroup can be easily obtained according to lookup table, which are given by $\{2, 3\}$ and $\{1, 4\}$, respectively. Similarly, the SAP and the complementary set of the second transmit antenna subgroup are given by $\{1, 3\}$ and $\{2, 4\}$, respectively. Finally, the transmit symbol matrix of the gth subblock is given by

$$\mathbf{X}^g = \begin{bmatrix} 0 & s & s & 0 \\ s & 0 & 0 & s \\ s & 0 & s & 0 \\ 0 & s & 0 & s \end{bmatrix} = \begin{bmatrix} \mathbf{x}^g_1 \\ \mathbf{x}^g_2 \\ \mathbf{x}^g_3 \\ \mathbf{x}^g_4 \end{bmatrix}, \tag{8}$$

$$\mathbf{X}^g = \left[\bar{\mathbf{x}}^g_1\ \bar{\mathbf{x}}^g_2\ \bar{\mathbf{x}}^g_3\ \bar{\mathbf{x}}^g_4\right], \tag{9}$$

Table 1: Reference SAPs lookup table with parameters $C\,4, 2$.

Bits	SAPs	Complementary set
[0, 0]	{1, 3}	{2, 4}
[0, 1]	{1, 4}	{2, 3}
[1, 0]	{2, 3}	{1, 4}
[1]	{2, 4}	{1, 3}

where $\mathbf{x}_t^g$ with $t = 1, 2, \cdots, 4$ in (8) denote the obtained transmitted symbol vectors in (4) and (5), and $\bar{\mathbf{x}}_n^g$ denotes the transmitted symbol vector corresponding to the nth subcarriers in the gth subblock, which is the data vector contains the simultaneously transmitted symbols from all the transmit antennas, and is the nth column vector in $\mathbf{X}^g$, $n = 1, 2, \cdots, 4$. According to IM method, the transmitted symbol vectors in (8) with odd indices of transmit antennas have K activated subcarriers, while the remaining with even indices have $N_S - K$ activated subcarriers. Furthermore, the transmitted symbol vectors $\mathbf{x}_t^g$ in (8) are the final output of IM in each transmit antenna level at the transmitter, while $\bar{\mathbf{x}}_n^g$ in (9) forms the basic signal demodulation model in subcarrier-wise detectors.

Similar to the SM systems, the AAPs are defined to denote the active statuses of $\bar{\mathbf{x}}_n^g$ in (9). To illustrate the AAPs more clarity, an example of AAPs with parameters $N_T = 4$ and $N_{TA} = 2$ is given in Table 2, and the number of the AAPs is given by $N_{\mathrm{AAP}} = 2^{N_{TA}}$. Let us define space-frequency activation patterns (SFAPs) set $\mathcal{X}$ to denote the active statuses of the transmitted symbol matrix $\mathbf{X}^g$, which is the combinations of the SAPs of each transmit antenna subgroups. Since the independent IM of each transmit antenna subgroups, there are a total of $N_{\mathrm{SFAP}} = (N_{\mathrm{SAP}})^{N_{TA}}$ SFAPs in the set $\mathcal{X}$. The SFAP of the transmitted symbol matrix in (8) is given by

$$\mathcal{X}^g = \begin{bmatrix} 0 & 1 & 1 & 0 \\ 1 & 0 & 0 & 1 \\ 1 & 0 & 1 & 0 \\ 0 & 1 & 0 & 1 \end{bmatrix}, \tag{10}$$

where 1 denotes the corresponding subcarrier is activated to transmit modulated symbol, while 0 denotes the inactive subcarrier.

2.2. Receiver. At the receiver, the time domain received signals are transformed to frequency signals by FFT operation in each branch after removing the CP samples. According to the signal model of MIMO, the received signals of the receiver antenna $r (1 \leqslant r \leqslant N_R)$ corresponding to the gth $(1 \leqslant g \leqslant G)$ subblock are given by

$$\mathbf{y}_r^g = \sum_{t=1}^{N_T} \gamma \,\mathrm{diag}\left(\mathbf{h}_{r,t}^g\right)\mathbf{x}_t^g + \mathbf{w}_r^g, \tag{11}$$

where $\mathbf{y}_r^g = [y_{r,1}^g, y_{r,2}^g, \cdots, y_{r,N_S}^g]^T$ denotes the $N_S \times 1$ received signal vector, $\gamma = \sqrt{N_S/K}$ is the power reallocation factor at the transmitter, $\mathbf{h}_r^g = [h_{r,t,1}^g, h_{r,t,2}^g, \cdots, h_{r,t,N_S}^g]^T$ denotes the $N_S \times 1$ channel frequency response between receive antenna r and transmit antenna t, and $\mathbf{w}_r^g = [w_{r,1}^g, w_{r,2}^g, \cdots, w_{r,N_S}^g]^T$ denotes the $N_S \times 1$ frequency additive white Gaussian noise (AWGN) vector with zero mean and N_0 variance. We define the signal to noise ratios (SNR) of the system as $r_{\mathrm{SNR}} = E_b/N_0$, where E_b is the average transmitted energy per bit. Owing to the orthogonality between different subcarriers in OFDM system, the calculation can be performed in subcarrier-wise within each subblock. According to the transmitted symbol vector model given in (9) and received signal model in (11), the received signal vector for the nth $(1 \leqslant n \leqslant N_S)$ subcarrier within the gth subblock can be expressed as

$$\begin{bmatrix} y_{1,n}^g \\ y_{2,n}^g \\ \vdots \\ y_{N_R,n}^g \end{bmatrix} = \gamma \begin{bmatrix} h_{1,1,n}^g & h_{1,2,n}^g & \cdots & h_{1,N_T,n}^g \\ h_{2,1,n}^g & h_{2,2,n}^g & \cdots & h_{2,N_T,n}^g \\ \vdots & \vdots & \ddots & \vdots \\ h_{N_R,1,n}^g & h_{N_R,2,n}^g & \cdots & h_{N_R,N_T,n}^g \end{bmatrix} \times \begin{bmatrix} x_{1,n}^g \\ x_{2,n}^g \\ \vdots \\ x_{N_T,n}^g \end{bmatrix} + \begin{bmatrix} w_{1,n}^g \\ w_{2,n}^g \\ \vdots \\ w_{N_T,n}^g \end{bmatrix},$$
$$\bar{\mathbf{y}}_n^g = \gamma \bar{\mathbf{H}}_n^g \bar{\mathbf{x}}_n^g + \bar{\mathbf{w}}_n^g \tag{12}$$

where $\bar{\mathbf{y}}_n^g$ is the $N_R \times 1$ received signal vector from all the receive antennas at the nth subcarrier, $\bar{\mathbf{H}}_n^g$ denotes the corresponding $N_R \times N_T$ channel matrix between the all the receive antennas and transmit antennas at the nth subcarrier, and $\bar{\mathbf{w}}_n^g$ denotes the $N_R \times 1$ AWGN vector. Due to the IM, only N_{TA} transmit antennas are activated to transmit nonzero modulated symbols, which can not be determined only based on the observation of current subcarrier. Therefore, the subcarrier-wise detection algorithms need to calculate the most likely transmitted symbol vectors corresponding to all the AAPs for each subcarrier within the subblock. Then, a joint decision is made based on the obtained most likely transmitted symbol vectors of N_S subcarriers. For the nth subcarrier, the subcarrier-wise ML detector calculates the most likely transmitted symbol vectors under the condition of each AAP

$$\hat{\bar{\mathbf{x}}}_{n,\mathscr{A}(a)}^g = \arg \min_{\bar{\mathbf{x}} \in \mathscr{A}(a)} \left\| \bar{\mathbf{y}}_n^g - \gamma \bar{\mathbf{H}}_n^g \bar{\mathbf{x}} \right\|^2, \tag{13}$$

where $a = 1, 2, \cdots, N_{\mathrm{AAP}}$, $\bar{\mathbf{x}} \in \mathscr{A}(a)$ denote all the possible transmitted symbol vectors whose AAP is $\mathscr{A}(a)$, and $\hat{\bar{\mathbf{x}}}_{n,\mathscr{A}(a)}^g$ denotes the obtained most likely transmitted symbol

Table 2: Reference AAPs for HE-MIMO-OFDM-IM with parameters $N_T = 4$ and $N_{TA} = 2$.

AAPs	$\mathscr{A}(1)$	$\mathscr{A}(2)$	$\mathscr{A}(3)$	$\mathscr{A}(4)$
Active state	$\begin{bmatrix} 0 \\ 1 \\ 0 \\ 1 \end{bmatrix}$	$\begin{bmatrix} 0 \\ 1 \\ 1 \\ 0 \end{bmatrix}$	$\begin{bmatrix} 1 \\ 0 \\ 0 \\ 1 \end{bmatrix}$	$\begin{bmatrix} 1 \\ 0 \\ 1 \\ 0 \end{bmatrix}$

vector corresponding to the AAP $\mathscr{A}(a)$. The metrics of the obtained most likely transmitted symbol vectors of the nth subcarrier can be expressed as

$$p\left(\widehat{\bar{\mathbf{x}}}^{g}_{n,\mathscr{A}(a)}\right) = \left\|\bar{\mathbf{y}}^{g}_{n} - \gamma\bar{\mathbf{H}}^{g}_{n}\widehat{\bar{\mathbf{x}}}^{g}_{n,\mathscr{A}(a)}\right\|^{2}. \tag{14}$$

After all the most likely transmitted symbol vectors of each subcarrier in the gth subblock are obtained, an exhaustive search of all the SFAPs is performed to obtained the final estimate of the transmitted symbol matrix, which can be calculated as

$$\widehat{\mathbf{X}}^{g} = \arg\min_{\mathscr{A}_n\in\mathscr{X}} \sum_{n=1}^{N_S} p\left(\widehat{\bar{\mathbf{x}}}^{g}_{n} \in \mathscr{A}_n\right), \tag{15}$$

where $\mathscr{A}_n$ denotes the AAP of the nth subcarrier which is the nth column of a given $\mathscr{X}$, and $\mathscr{A}_n \in \{\mathscr{A}(1), \mathscr{A}(2), \cdots, \mathscr{A}(N_{\mathrm{AAP}})\}$. Although the subcarrier-wise ML detector can achieve the optimal error performance, both the detection complexity in the first step and the second step increase exponentially with the order of constellation and SAPs, which are given by $\mathcal{O}(M^{N_{TA}})$ and $\mathcal{O}((N_{\mathrm{SAP}})^{N_{TA}})$, respectively. The demodulation complexity in terms of the FLOPs to get the estimate of the transmitted symbol matrix per subcarrier is given by

$$(3N_R N_T + 2N_R - 1)M^{N_{TA}}N_{\mathrm{AAP}} + (N_S - 1)(N_{\mathrm{SAP}})^{N_{TA}}. \tag{16}$$

3. Low-Complexity Detector

The computational complexity of the optimal ML detector increases exponentially with the order of the constellation and the number of the transmit antenna subgroups, which give rise to prohibitive computational complexity in the practical applications in the mMTC scenario. In this section, a novel two-step SMC detector is proposed to reduce detection complexity. In the first step, a null space algorithm is proposed to calculate the metrics of the AAPs of each subcarrier, which can be used to calculate the most likely transmitted SFAPs of the subblock. Then, the most likely transmitted symbol vectors of each subcarrier can be calculated according to the obtained SFAPs. Before the detection, we first calculate the noise whitening matrix of the nth $(1 \leqslant n \leqslant N_S)$ subcarrier, which is given by

$$\mathbf{\Omega}^{g}_{n} = \left(\left(\bar{\mathbf{H}}^{g}_{n}\right)^{H}\bar{\mathbf{H}}^{g}_{n}\right)^{1/2}. \tag{17}$$

The output after the signal processing of noise whitening is given by

$$\begin{aligned}\bar{\mathbf{y}}^{g}_{n,NW} &= \left(\mathbf{\Omega}^{g}_{n}\right)^{-1}\left(\bar{\mathbf{H}}^{g}_{n}\right)^{H}\bar{\mathbf{y}}^{g}_{n}\\ &= \gamma\left(\left(\bar{\mathbf{H}}^{g}_{n}\right)^{H}\bar{\mathbf{H}}^{g}_{n}\right)^{-1/2}\left(\bar{\mathbf{H}}^{g}_{n}\right)^{H}\bar{\mathbf{H}}^{g}_{n}\bar{\mathbf{x}}^{g}_{n} + \left(\mathbf{\Omega}^{g}_{n}\right)^{-1}\left(\bar{\mathbf{H}}^{g}_{n}\right)^{H}\bar{\mathbf{w}}^{g}_{n}\\ &= \gamma\left(\left(\bar{\mathbf{H}}^{g}_{n}\right)\bar{\mathbf{H}}^{g}_{n}\right)^{1/2}\bar{\mathbf{x}}^{g}_{n} + \left(\mathbf{\Omega}^{g}_{n}\right)^{-1}\left(\bar{\mathbf{H}}^{g}_{n}\right)^{H}\bar{\mathbf{w}}^{g}_{n} = \gamma\mathbf{\Omega}^{g}_{n}\bar{\mathbf{x}}^{g}_{n} + \bar{\mathbf{w}}^{g}_{n,NW},\end{aligned} \tag{18}$$

where $\bar{\mathbf{y}}^{g}_{n,NW}$ denotes the $N_T \times 1$ received signal vector after the signal processing and $\bar{\mathbf{w}}^{g}_{n,NW}$ denotes the processed $N_T \times 1$ AWGN sample vector. Since IM is performed in each branch, there are some inactive antennas in each subcarrier, which indicates that there are some 0 symbols in $\bar{\mathbf{x}}^{g}_{n}$. Assume the AAP of the nth subcarrier is $\mathscr{A}_n$, the formula in (18) can be rewritten as

$$\bar{\mathbf{y}}^{g}_{n,NW} = \gamma\mathbf{\Omega}^{g}_{n,\mathscr{A}_n}\bar{\mathbf{x}}^{g}_{n,\mathscr{A}_n} + \bar{\mathbf{w}}^{g}_{n,NW}, \tag{19}$$

where $\mathbf{\Omega}^{g}_{n,\mathscr{A}_n}$ denotes the submatrix with dimension $N_T \times N_{TA}$ that deletes the columns corresponding to the inactive subcarriers in $\mathscr{A}_n$ and $\bar{\mathbf{x}}^{g}_{n,\mathscr{A}_n}$ denotes the $N_{TA} \times 1$ modulated symbol vector by deleting the zero symbols in $\bar{\mathbf{x}}^{g}_{n}$ according to its AAP $\mathscr{A}_n$. By performing the QR decomposition of the matrix $\mathbf{\Omega}^{g}_{n,\mathscr{A}_n}$, the result can be expressed as

$$\mathbf{\Omega}^{g}_{n,\mathscr{A}_n} = \left[\mathbf{Q}^{g}_{\alpha,n,\mathscr{A}_n}, \mathbf{Q}^{g}_{\beta,n,\mathscr{A}_n}\right]\begin{bmatrix}\left(\mathbf{R}^{g}_{\alpha,n,\mathscr{A}_n}\right)_{N_{TA}\times N_{TA}}\\ \mathbf{0}_{(N_T - N_{TA})\times N_{TA}}\end{bmatrix} = \mathbf{Q}^{g}_{\alpha,n,\mathscr{A}_n}\mathbf{R}^{g}_{\alpha,n,\mathscr{A}_n}, \tag{20}$$

where $\mathbf{Q}^{g}_{\alpha,n,\mathscr{A}_n}$ is an $N_T \times N_{TA}$ unitary matrix, $\mathbf{Q}^{g}_{\beta,n,\mathscr{A}_n}$ is the null space matrix with dimension $N_T \times (N_T - N_{TA})$, and $\mathbf{R}^{g}_{\alpha,n,\mathscr{A}_n}$ is an $N_{TA} \times N_{TA}$ upper triangular matrix. From (20), we have

$$\left(\mathbf{Q}^{g}_{\beta,n,\mathscr{A}_n}\right)^{H}\mathbf{\Omega}^{g}_{n,\mathscr{A}_n} = \mathbf{0}, \tag{21}$$

which implies that $\left(\mathbf{Q}^{g}_{\beta,n,\mathscr{A}_n}\right)^{H}$ is orthogonal to the matrix $\mathbf{\Omega}^{g}_{n,\mathscr{A}_n}$. By left multiply $\left(\mathbf{Q}^{g}_{\beta,n,\mathscr{A}_n}\right)^{H}$ to the received signal victor $\bar{\mathbf{y}}^{g}_{n,NW}$ given in (18), the output can be expressed as

$$\bar{\mathbf{y}}^{g}_{n,C} = \left(\mathbf{Q}^{g}_{\beta,n,\mathscr{A}_n}\right)^{H}\bar{\mathbf{y}}^{g}_{n,NW} = \gamma\left(\mathbf{Q}^{g}_{\beta,n,\mathscr{A}_n}\right)^{H}\mathbf{\Omega}^{g}_{n,\mathscr{A}_n}\bar{\mathbf{x}}^{g}_{n,\mathscr{A}_n} + \left(\mathbf{Q}^{g}_{\beta,n,\mathscr{A}_n}\right)^{H}\bar{\mathbf{w}}^{g}_{n,NW}. \tag{22}$$

If $\mathbf{Q}^{g}_{\beta,n,\mathscr{A}_n}$ is the correct null space matrix, the result of (22) can be expressed as $\bar{\mathbf{y}}^{g}_{n,C} = \left(\mathbf{Q}^{g}_{\beta,n,\mathscr{A}_n}\right)^{H}\bar{\mathbf{w}}^{g}_{n,NW}$, which follows zero mean Gaussian distribution; otherwise, the transmitted symbol vectors are nonorthogonal to the null space and the output will be nonzero mean variables. Therefore, $\left\|\bar{\mathbf{y}}^{g}_{n,C}\right\|^{2}$ can be used as the metrics for the detection of the possible AAPs of each subcarrier and the SFAPs of each subblock. Let us define $\varphi^{g}_{n}(\mathscr{A}(a))$ to denotes the metric of the n th subcarrier corresponding to the AAP $\mathscr{A}(a)$, which is given by

$$\varphi^{g}_{n}(\mathscr{A}(a)) = \left\|\left(\mathbf{Q}^{g}_{\beta,n,\mathscr{A}(\alpha)}\right)^{H}\bar{\mathbf{y}}^{g}_{n,NW}\right\|^{2}, \tag{23}$$

where $\mathbf{Q}^{g}_{\beta,n,\mathscr{A}(\alpha)}$ denotes the null space of the nth subcarrier obtained from the submatrix $\mathbf{\Omega}^{g}_{n,\mathscr{A}(a)}$ which is generated by

deleting the columns corresponding to the inactive subcarriers according to $\mathscr{A}(a)$, $a = 1, 2, \cdots, N_{\mathrm{AAP}}$.

After the calculation of N_S subcarriers within the gth subblock, the estimate of SFAP can be obtained by using a SD-like algorithm to find the most likely transmitted SFAPs of the subblock in the subcarrier to subcarrier manner based on the metrics obtained in (23). Considering there are some illegal SAPs in IM in each branch, which will lead to catastrophic errors both in the demodulation of IM bits and the location of the modulated symbols as well as their order. Therefore, we need to check the validity of the SAP of each transmit antenna subgroup during the searching process. The SD-like algorithm can be performed in several steps as follows.

Step 1: let us define $\widehat{\mathscr{X}}^g_{n,k}$ to denote the survival partial SFAPs reach the nth $(1 \leqslant n \leqslant N_S - 1)$ subcarrier level, where the kth survival partial SFAPs can be expressed as

$$\widehat{\mathscr{X}}^g_{n,k} = \left[\mathscr{A}^g_{1,k}, \mathscr{A}^g_{2,k}, \cdots, \mathscr{A}^g_{n,k}\right], \tag{24}$$

where $\mathscr{A}^g_{n,k}$ denotes the AAP at the nth subcarrier in the kth survival partial SFAPs $\widehat{\mathscr{X}}^g_{n,k}$, $k = 1, 2, \cdots, \theta_A$ denotes the index of the survival partial SFAPs and θ_A is the maximum number of the reserved survival partial SFAPs at each subcarrier level. The corresponding cumulative metrics of the partial SFAPs can be calculated as

$$\varphi\left(\widehat{\mathscr{X}}^g_{n,k}\right) = \sum_{i=1}^{n} \varphi^g_i\left(\mathscr{A}^g_{i,k}\right), \tag{25}$$

where $\varphi^g_i(\mathscr{A}^g_{i,k})$ denotes the metric at ith subcarrier corresponding to the AAP in the kth survival partial SFAP $\widehat{\mathscr{X}}^g_{n,k}$. Then, the partial SFAPs of the $(n+1)$th subcarrier can be directly calculated based on the obtained calculation results in (24) and (25).

Step 2: the entire partial SFAPs at the $(n+1)$th subcarrier level based on the obtained results in (24) and (25) can be expressed as

$$\widehat{\mathscr{X}}^g_{n+1,l} = \left[\widehat{\mathscr{X}}^g_{n,k}, \mathscr{A}(a)\right] = \left[\mathscr{A}^g_{1,k}, \mathscr{A}^g_{2,k}, \cdots, \mathscr{A}^g_{n,k}, \mathscr{A}(a)\right], \tag{26}$$

where $l = 1, 2, \cdots, \theta_A N_{\mathrm{AAP}}$ is the index of entire partial SFAPs at the $(n+1)$th subcarrier level, $k = 1, 2, \cdots, \theta$, $a = 1, 2, \cdots, N_{\mathrm{AAP}}$. The cumulative metrics of the partial SFAPs in (26) can be obtained by updating the metrics in (25), which can be calculated as

$$\varphi\left(\widehat{\mathscr{X}}^g_{n+1,l}\right) = \varphi\left(\widehat{\mathscr{X}}^g_{n,k}\right) + \varphi^g_{n+1}(\mathscr{A}(a)). \tag{27}$$

After this point, θ_A partial SFAPs with better metrics are kept as the survival partial SFAPs at the $(n+1)$th subcarrier level for the calculation of the next subcarrier level. In this process, we need to check the validity of the SFAPs of each transmit antenna subgroup, which can be actualized with the aid of an illegal SAP table at each subcarrier level. An example of the illegal SAPs table of each subcarrier level corresponding to the SAPs given in Table 1 is given in Table 3. The obtained survival SFAPs and the corresponding metrics are given by

$$\widehat{\mathscr{X}}^g_{n+1,k} = \left[\mathscr{A}^g_{1,k}, \mathscr{A}^g_{2,k}, \cdots, \mathscr{A}^g_{n,k}, \mathscr{A}^g_{n+1,k}\right], \tag{28}$$

$$\varphi\left(\widehat{\mathscr{X}}^g_{n+1,k}\right) = \sum_{i=1}^{n+1} \varphi^g_i\left(\mathscr{A}^g_{i,k}\right), \tag{29}$$

respectively, where the index k is given by $k = 1, 2, \cdots, \theta_A$. Note that although the formulae expresses in (28) and (29) have the same form as that in (24) and (25), the elements in them may different even with same index k because some partial SFAPs may be eliminated due to the metrics in (27). Finally, let us set $n_{\mathrm{current}} = n + 1$ and check whether the search process reach the last subcarrier level. If $n_{\mathrm{current}} = N_S$, go to Step 3 for the following demodulation procedures; otherwise set $n = n_{\mathrm{current}}$ and repeat Step 2.

Step 3: when it arrives the last subcarrier level, θ_F SFAPs with better metrics are selected as the most likely transmitted SFAPs for the calculation of the modulated symbols, which are given by

$$\widehat{\mathscr{X}}^g_{N_S,c} = \left[\mathscr{A}^g_{1,c}, \mathscr{A}^g_{2,c}, \cdots, \mathscr{A}^g_{N_S,c}\right], \tag{30}$$

where $c = 1, 2, \cdots, \theta_F$. For convenience of expression, let us define $\mathscr{X}^g_n = \{\mathscr{A}^g_{n,1}, \mathscr{A}^g_{n,2}, \cdots \mathscr{A}^g_{n,\theta_F}\}$ to denote the set of the AAPs of the$n$th subcarrier in $\widehat{\mathscr{X}}^g_{N_S,c}$, $n = 1, 2, \cdots, N_S$.

According to the obtained AAP set of the nth subcarrier, the most likely transmitted symbol vectors can be calculated based on the SMC theory. Note that the AAPs of each subcarrier may identical in different SFAP estimates, the most likely transmitted symbol vectors corresponding to these AAPs are only needed to be calculated once. For a given AAP $\mathscr{A}^g_{n,c}$, the noising submatrix $\mathbf{\Omega}^g_{n,\mathscr{A}^g_{n,c}}$ which only keeps the columns corresponding to the activated transmit antennas according to the AAP $\mathscr{A}^g_{n,c}$. Then, QR decomposition given in (20) is perform to get the demodulation signal model for SMC calculation. Consequently, we have

$$\bar{\mathbf{y}}^g_{n,c} = \left(\mathbf{Q}^g_{\alpha,n,\mathscr{A}^g_{n,c}}\right)^H \bar{\mathbf{y}}^g_{n,NW} = \gamma \mathbf{R}^g_{\alpha,n,\mathscr{A}^g_{n,c}} \bar{\mathbf{x}}^g_{n,c} + \left(\mathbf{Q}^g_{\alpha,n,\mathscr{A}^g_{n,c}}\right)^H \bar{\mathbf{w}}^g_{n,NW}, , \tag{31}$$

where $\bar{\mathbf{x}}^g_{n,c}$ denotes the nonzero modulated symbol vector of the transmitted symbol vector $\bar{\mathbf{x}}^g_n$ corresponding to the AAP $\mathscr{A}^g_{n,c}$. Formula (31) can be rewritten in matrix wise

$$\begin{bmatrix} y_{1,n} \\ y_{2,n} \\ \vdots \\ y_{K,n} \end{bmatrix} = \gamma \begin{bmatrix} r_{1,1} & r_{1,2} & \cdots & r_{,1K} \\ 0 & r_{2,2} & \cdots & r_{2,K} \\ 0 & \vdots & \ddots & \vdots \\ 0 & 0 & \cdots & r_{K,K} \end{bmatrix} \begin{bmatrix} s_1 \\ s_2 \\ \vdots \\ s_K \end{bmatrix} + \begin{bmatrix} \bar{w}_1 \\ \bar{w}_2 \\ \vdots \\ \bar{w}_K \end{bmatrix}. \tag{32}$$

Table 3: Illegal paths table for OFDM-IM with parameters $C\,4, 2$.

Subcarrier level	Illegal paths
Subcarrier 1	∅
Subcarrier 2	[0 0], [1 1]
Subcarrier 3	∅
Subcarrier 4	[0 1 0 0], [0 1 1 1] [1 0 0 0], [1 0 1 1]

According to the SMC theory, the detection process of the most likely transmitted symbol vectors associated with $\mathscr{A}^g_{n,c}$ can be performed in antenna to antenna manner from the Kth activated transmit antenna to the first activated transmit antenna. Based on the sequential distribution and the sequential structure derived in [48], the *a posteriori* probability at the kth activated transmit antenna level can be calculated as

$$\begin{aligned} p\left(\left\{\bar{\mathbf{s}}^g_{n,c}\right\}_k \middle| \left\{\bar{\mathbf{y}}^g_{n,c}\right\}_k\right) &\propto p\left(\left\{\bar{\mathbf{y}}^g_{n,c}\right\}_k \middle| \left\{\bar{\mathbf{s}}^g_{n,c}\right\}_k\right) \\ &\propto \prod_{t=K}^{k} p\left(y^g_{t,n} \middle| \left\{\bar{\mathbf{s}}^g_{n,c}\right\}_t\right) \propto p\left(\left\{\bar{\mathbf{y}}^g_{n,c}\right\}_{k+1} \middle| \left\{\bar{\mathbf{s}}^g_{n,c}\right\}_{k+1}\right) p\left(y^g_{k,n} \middle| \left\{\bar{\mathbf{s}}^g_{n,c}\right\}_k\right), \end{aligned} \tag{33}$$

where $\{\bar{\mathbf{s}}^g_{n,c}\}_k \triangleq [s_k, s_{k+1}, \cdots, s_K]^T$ is the partial symbol vector when the calculation reaches the kth activated transmit antenna level and $\{\bar{\mathbf{y}}^g_{n,c}\}_k \triangleq [y_k, y_{k+1}, \cdots, y_K]^T$ denotes the partial receive signal vector reaches the kth activated transmit antenna level. For the calculation of each activated transmit antenna level, we define the $(K-k+1)\times 1$ nonzero vector $\mathbf{r}_k = [r_{k,k}, r_{k,k+1}, \cdots r_{k,K}]$ to denote the vector which is constructed by $K-k+1$ nonzero elements in the kth row of the matrix $\mathbf{R}^g_{\alpha,n,\mathscr{A}^g_{n,c}}$. Therefore, the SMC algorithm draws particles from each activated transmit antenna level and keeps θ_S particles according to the probabilities in (33) for the calculation of the next antenna level. After the calculation of the kth activated transmit antenna level, θ_S reserved particles can be expressed as $\{\bar{\mathbf{s}}^g_{n,c}\}^{(\theta)}_k$ with their important weights $p(\{\bar{\mathbf{y}}^g_{n,c}\}_k | \{\bar{\mathbf{s}}^g_{n,c}\}^{(\theta)}_k)$, where $\theta = 1, 2, \cdots, \theta_S$. In the SMC algorithm, the particles at the $(k-1)$th activated transmit antenna level can be expressed as

$$\left\{\bar{\mathbf{s}}^g_{n,c}\right\}^{(l)}_{k-1} = \left[s_{k-1}, \left(\left\{\bar{\mathbf{s}}^g_{n,c}\right\}^{(\theta)}_k\right)^T\right]^T, \tag{34}$$

where $l = 1, 2, \cdots M\theta_S$. Note that all the particles at the $(k-1)$th activated transmit antenna level are updated from θ_S particles at the kth activated transmit antenna level, which indicates that the important weights can be updated from that of the kth activated transmit antenna level. The updating of the important weights at the next antenna level, which is performed based of the important weights of the obtained θ_S particles, can be calculated as

$$p\left(\left\{\bar{\mathbf{y}}^g_{n,c}\right\}_{k-1} \middle| \left\{\bar{\mathbf{s}}^g_{n,c}\right\}^{(l)}_{k-1}\right) \propto p\left(\left\{\bar{\mathbf{y}}^g_{n,c}\right\}_k \middle| \left\{\bar{\mathbf{s}}^g_{n,c}\right\}^{(\theta)}_k\right) p\left(y^g_{k-1,n} \middle| \left\{\bar{\mathbf{s}}^g_{n,c}\right\}^{(l)}_{k-1}\right). \tag{35}$$

When it reaches the first activated transmit antenna level, the final θ_S particles can be expressed as $\{\bar{\mathbf{s}}^g_{n,c}\}^{(\theta)}_1$ with $\theta = 1, 2, \cdots, \theta_S$. The complete θ_S symbol vectors can be generated directly by mapping the obtained particles $\{\bar{\mathbf{s}}^g_{n,c}\}^{(\theta)}_1$ to the nonzero indices according to the AAP $\mathscr{A}^g_{n,c}$, which are given by $\{\bar{\mathbf{x}}^g_{n,c}\}^{(\theta)}$. Then, the most likely transmitted symbol vector of the nth subcarrier corresponding to the AAP $\mathscr{A}^g_{n,c}$ can be calculated based on the signal model given in (18)

$$\hat{\bar{\mathbf{x}}}^g_{n,\mathscr{A}^g_{n,c}} = \arg \min_{\bar{\mathbf{x}} \in \left\{\bar{\mathbf{x}}^g_{n,c}\right\}^{(\theta)}} \left\| \bar{\mathbf{y}}^g_{n,NW} - \gamma \boldsymbol{\Omega}^g_n \bar{\mathbf{x}} \right\|^2, \tag{36}$$

and the corresponding decision metric is given by

$$p\left(\hat{\bar{\mathbf{x}}}^g_{n,\mathscr{A}^g_{n,c}}\right) = \left\| \bar{\mathbf{y}}^g_{n,NW} - \gamma \boldsymbol{\Omega}^g_n \hat{\bar{\mathbf{x}}}^g_{n,\mathscr{A}^g_{n,c}} \right\|^2. \tag{37}$$

The final SFAP estimate of the gth subblock can be calculated based on the metrics of most likely transmitted symbol vectors of the AAPs in $\hat{\mathscr{X}}^g_{N_S,c}$

$$\hat{\mathscr{X}}^g = \arg \min_{\hat{\mathscr{X}}^g_{N_S,c}} \sum_{n=1}^{N_S} p\left(\hat{\bar{\mathbf{x}}}^g_{n,\mathscr{A}^g_{n,c}}\right), \tag{38}$$

where $c = 1, 2, \cdots, \theta_F$. After this point, the obtained final SFAP can be expressed as

$$\hat{\mathscr{X}}^g = \left[\mathscr{A}^g_1, \mathscr{A}^g_2, \cdots, \mathscr{A}^g_{N_S}\right]. \tag{39}$$

Finally, the estimate of the transmitted symbol matrix can be obtained by concatenating the most likely symbol vectors of each subcarrier in (36) according to the final SFAP estimate $\hat{\mathscr{X}}^g$, which is given by

$$\hat{\mathbf{X}}^g = \left[\hat{\bar{\mathbf{x}}}^g_{1,\mathscr{A}^g_1}, \hat{\bar{\mathbf{x}}}^g_{2,\mathscr{A}^g_2}, \cdots, \hat{\bar{\mathbf{x}}}^g_{N_S,\mathscr{A}^g_{N_S}}\right]. \tag{40}$$

The computational complexity in terms of the FLOPs of the SMC detector can be obtained according to the above formulae. Since the repetitions of AAPs in the different obtained SFAPs are difficult to count, we omit it in the following computational complexity analysis. The computational complexity in terms of the FLOPs to get the final estimate of the transmitted symbol matrix per subcarrier is less than

$$\begin{aligned} &N_{\mathrm{AAP}}(2N_{TA}N_T - N_{TA} + \theta_A + 1) \\ &\quad + N_T(2N_TN_R + N_R - 1) + \theta_F(2\theta_S N_T(N_T + 1)) \\ &\quad + \theta_F\left(2N_T(N_{TA} - 1) + \theta_S M\left((N_{TA})^2 + 3N_{TA}\right)\right). \end{aligned} \tag{41}$$

From the above analysis, the computational complexity of a given system is affected by the parametersθ_F and θ_S, which

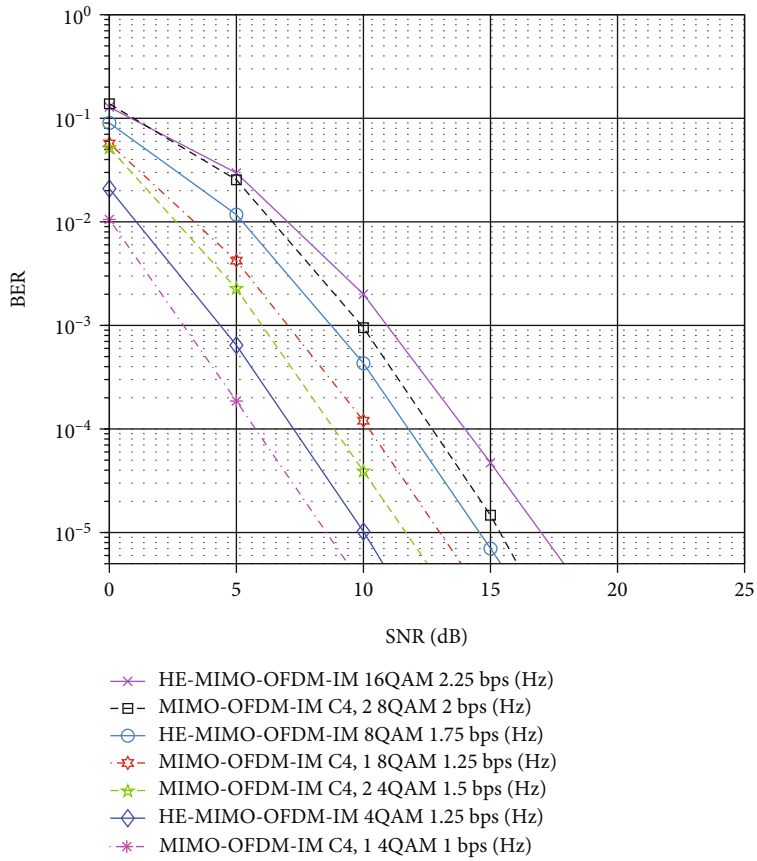

Figure 3: Error performance comparison of conventional MIMO-OFDM-IM and HE-MIMO-OFDM-IM with optimal ML detectors.

indicates that an interesting trade-off between the system error performance and demodulation complexity can be realized by adjusting these parameters.

4. Simulation Results

In this section, we perform Monte Carlo simulations to verify the error performance of HE-MIMO-OFDM-IM with different parameters. The MIMO configuration in simulations is given by $N_T = 4$ and $N_R = 4$. The length of the OFDM bloc is given by $N = 128$, and the length of CP is $N_{\mathrm{CP}} = 16$. In HE-MIMO-OFDM-IM, the parameters of IM in each subblock are given by $C4, 2$. In the computer simulations, uncoded transmission is considered over frequency-selective Rayleigh fading MIMO channels, whose maximum delay spread is less than 12 sampling periods. It is assumed that the receiver estimates the perfect channel state information, which is unknown at the transmitter. Here, we use MMSE-LLR to denote the proposed low-complexity MMSE-LLR detector for MIMO-OFDM-IM in [44] and HSMC detector to denote the SMC detector proposed in [47], which can also be employed in the proposed HE-MIMO-OFDM-IM scheme.

Figure 3 compares the BER performance between conventional MIMO-OFDM-IM and HE-MIMO-OFDM-IM with constellations 4QAM, 8QAM, and 16QAM by employing the optical ML detector. Since the computation complexity of the ML detector of MIMO-OFDM-IM with constellation 16QAM is too high, the corresponding curve is not provided in Figure 3. It is observed in Figure 3 that HE-MIMO-OFDM-IM outperforms conventional MIMO-OFDM-IM with same constellation and IM parameters due to the transmit diversity achieved by the HE-MIMO-OFDM-IM scheme. According to the principle of IM, p_1 index bits occupies only a small percentage in the p total bits because small size of subblock is needed to maintain low complexity in both modulation and demodulation. In particularly, there are total $p = 10$ bits per subblock in MIMO-OFDM-IM when 16QAM employed and the proposed scheme suffers only one bits loss per subblock, the percentage of loss decreases as the order of constellation increases because the loss of index bits do not change with the order of the constellation. By reducing the number of the activated subcarriers in the subblock, i.e., $K = 1$, the proposed HE-MIMO-OFDM-IM outperforms conventional MIMO-OFDM-IM with the same SE. Note that, the computation complexity in the calculation of the most likely transmitted symbol vectors for each subcarrier does not change with the number of the activated subcarriers K in conventional MIMO-OFDM-IM. Combining with the demodulation complexity comparison in Figure 4, the proposed HE-MIMO-OFDM-IM achieves extremely low detection complexity when higher-order constellations are employed. Therefore, low detection complexity and gradually diminished SE loss in higher-order constellations applications

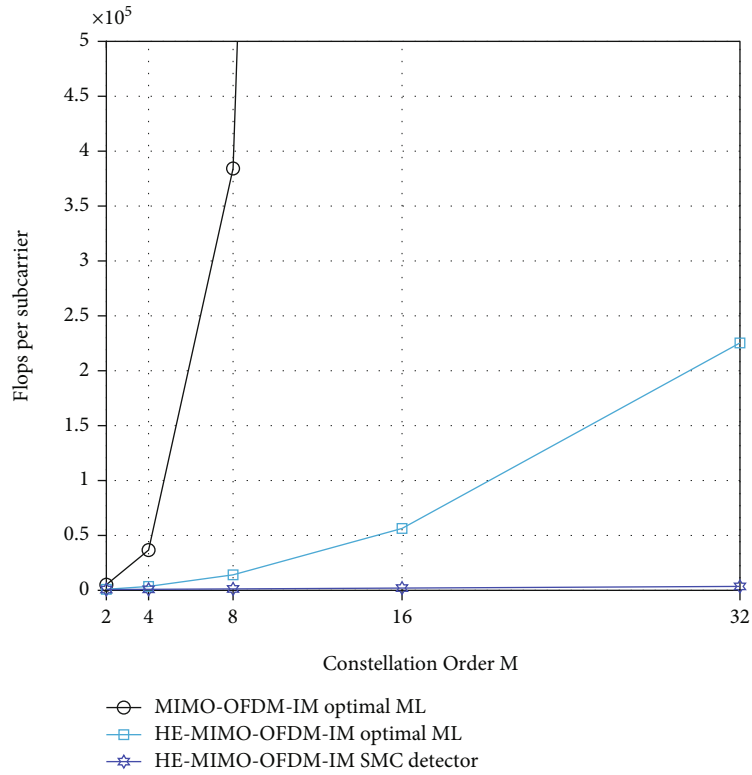

Figure 4: Flops comparison of different detectors for conventional MIMO-OFDM-IM and HE-MIMO-OFDM-IM.

make the proposed HE-MIMO-OFDM-IM becomes a competitive alternative to conventional MIMO-OFDM-OFDM.

Figure 4 compares the computational complexity in terms of the flops for the optimal ML detectors for both MIMO-OFDM-IM and HE-MIMO-OFDM-IM, the SMC detector with parameter $\theta_A = \theta_F = 4$ and $\theta_S = 5$ for HE-MIMO-OFDM-IM. In comparisons, 4×4 MIMO configuration is considered. The OFDM-IM parameters in comparison are given by $N_S = 4$ and $K = 2$. Due to there are some identical AAPs in θ_F final SFAPs at the same subcarrier level, the computational complexity of the SMC detector is obtained by the computer simulations. As shown in Figure 4, the computational complexity of the optimal ML detector for HE-MIMO-OFDM-IM is less than that of MIMO-OFDM-IM, which validates that the proposed scheme has potential to meet the request of low-complexity implementation scenarios. This can be explained that the proposed HE-MIMO-OFDM-IM has only $2^{N_{TA}}$ AAPs which have N_{TA} nonzero symbols, while MIMO-OFDM-IM has 2^{N_T} AAPs in which the nonzero symbols range from 0 to N_T. The SMC detector can further reduce the demodulation complexity by exploiting the null space to calculate the most likely transmitted SFAPs and calculates the most likely transmitted symbol vectors by using the SMC algorithm in the second step. Furthermore, other low-complexity detection algorithms can be used to substitute the SMC algorithm after the null space calculations in the second step, which can further reduce the demodulation complexity for high-order MIMO configurations.

Figure 5 compares the BER performance of different detectors for HE-MIMO-OFDM-IM with 4QAM and 16QAM constellations. The number of the survival partial SFAPs of each subcarrier level in the proposed SMC detector is given by $\theta_A = \theta_F = 4$ and the number of the particles in the SCM algorithm is given by $\theta_S = 5$. The number of the particles in the HSMC detector for 4QAM and 16QAM constellations are given by $\theta_S = 6$ and $\theta_S = 13$, respectively, and the survival paths in the SD-like algorithm to get the estimate of the submatrix is given by $\theta_{\text{path}} = 8$. Because there are some illegal AAPs, a validity check of the AAPs in the calculation of the most likely transmitted symbol vectors is needed in the HSMC detector. The MMSE-LLR detector suffers from a significant error performance degradation compared with the optimal ML detector and the proposed SMC detector due to only one receive diversity order achieved. As shown in Figure 5, all the SMC detectors achieve near-optimal BER performance with the reduced computational complexity, which indicates that the SMC detectors achieve the diversity order N_R as that of the optimal ML detector. In particularly, the proposed SMC detector has potential to achieve almost the same BER performance as that of the optimal ML detector in the medium to high SNRs, which demonstrate that the null space method can effectively acquire almost the same SFAP estimate as that of the optimal ML detector if enough partial SFAPs are kept at each subcarrier level in the calculations. This phenomenon indicates that two-step detection algorithm, in which the first step uses the null space method to get the most

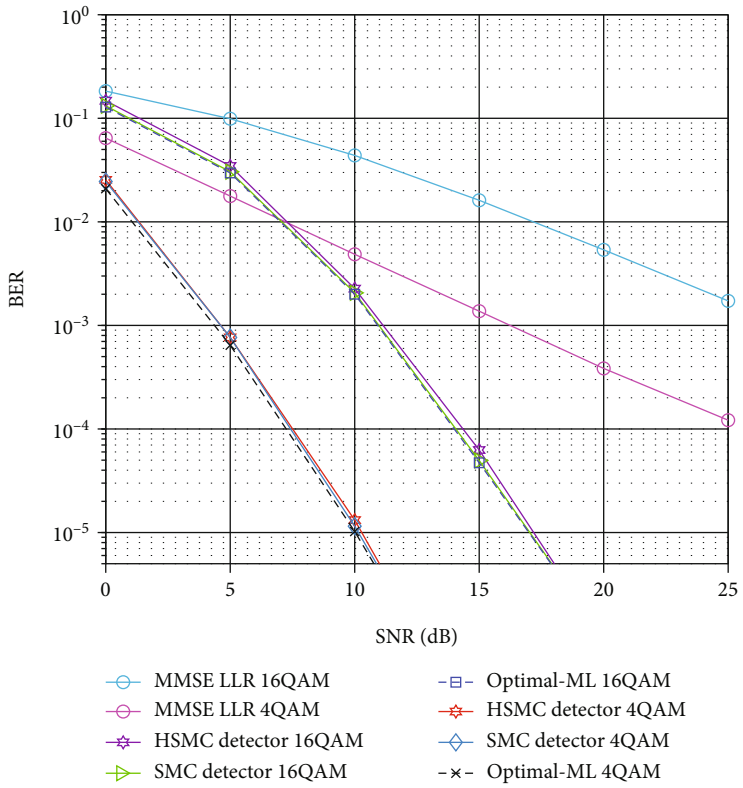

Figure 5: Error performance comparison of different detectors for HE-MIMO-OFDM-IM.

likely transmitted SFAPs and the second step detects the modulated symbol vectors based the results in the first step, can be a valuable method for the IM-aided MIMO systems. Furthermore, the SMC detector can achieve a trade-off between error performance, system SE, and demodulation complexity by adjusting the corresponding parameters to meet the requests of different scenarios.

5. Conclusion

In this paper, we have proposed a novel HE-MIMO-OFDM-IM scheme which performs IM in each transmit antenna subgroup to achieve two transmit diversity order of IM patterns and achieves extremely low computational complexity at the receiver side. Then, the subcarrier-wise ML detector, which is performed in two steps, is proposed for HE-MIMO-OFDM-IM. Due to the fixed number of the activated transmit antennas at each subcarrier level, the null space submatrix of the QR decomposition of the noise whitening preprocessed channel response matrix can be used to calculate the most likely transmitted IM patterns of each sub-block. Then, a novel SMC detector is proposed to exploit the null space submatrix to calculate the most likely transmitted SFAPs first and then calculates the most likely transmitted symbol vectors of each subcarrier based on the SMC theory according to the obtained most likely transmitted SFAPs. The computer simulation results have shown that the proposed HE-MIMO-OFDM-IM achieves better BER performance under same constellation at cost of a minor SE and achieves extremely low demodulation complexity compared with that of conventional MIMO-OFDM-IM. Consequently, the advantages in error performance and computational complexity makes the proposed HE-MIMO-OFDM-IM more favorable to the mMTC scenarios.

Data Availability

No data were used to support this study.

Conflicts of Interest

The authors declare that there is no conflict of interest regarding the publication of this paper.

Acknowledgments

This work was funded in part by the National Natural Science Foundation of China (grant numbers 62071504, 61971149, and 61971198), in part by the Joint Fund of National Natural Science Foundation of China and Zhejiang Province (grant number U1809211), in part by the Guangdong Basic and Applied Basic Research Foundation (grant number 2021A1515011657 and 2020A1515110958), in part by the Special Foundation in Key Fields for Colleges and Universities of Guangdong Province (New Generation of Information Technology) (grant number 2020ZDZX3025), and in part by the Shaanxi Provincial Natural Science Foundation (grant number 2021JQ-486), in part by the Key-Area Research and Development Program of Guangdong

Province (grant number 2020B1111010002).The authors would also like to acknowledge the support of the School of Electronic and Information Engineering, South China University of Technology.

References

[1] H. Tataria, M. Shafi, A. F. Molisch, M. Dohler, H. S. Oland, and F. Tufvesson, "6G wireless systems: vision, requirements, challenges, insights, and opportunities," *Proceedings of the IEEE*, vol. 109, no. 7, pp. 1166–1199, 2021.

[2] M. Z. Chowdhury, M. Shahjalal, S. Ahmed, and Y. M. Jang, "6G wireless communication systems: applications, requirements, technologies, challenges, and research directions," *IEEE Open Journal of the Communications Society*, vol. 1, pp. 957–975, 2020.

[3] E. Memisoglu, E. Basar, and H. Arslan, "Fading-aligned OFDM with index modulation for mMTC services," *Physical Communication*, vol. 35, p. 100680, 2019.

[4] Q. Liu, S. Sun, H. Wang, and S. Zhang, "6G green IoT network: joint design of intelligent reflective surface and ambient backscatter communication," *Wireless Communications and Mobile Computing*, vol. 2021, 2031 pages, 2021.

[5] J. Lin, W. Yu, N. Zhang, X. Yang, H. Zhang, and W. Zhao, "A survey on internet of things: architecture, enabling technologies, security and privacy, and applications," *IEEE Internet of Things Journal*, vol. 4, no. 5, pp. 1125–1142, 2017.

[6] M. Wen, S. Lin, K. J. Kim, and F. Ji, "Cyclic delay diversity with index modulation for green internet of things," *IEEE Transactions on Green Communications and Networking*, vol. 5, no. 2, pp. 600–610, 2021.

[7] R. S. Biljana, T. Kire, and D. Danco, "Internet of things framework for home care systems," *Wireless Communications and Mobile Computing*, vol. 2017, 10 pages, 2017.

[8] S. R. Pokhrel, J. Ding, J. Park, O.-S. Park, and J. Choi, "Towards enabling critical mMTC: a review of URLLC within mMTC," *IEEE Access*, vol. 8, pp. 131796–131813, 2020.

[9] M. Wen, X. Cheng, and L. Yang, *Index Modulation for 5G Wireless Communications*, Springer International Publishing AG, Cham, Switzerland, 2017.

[10] E. Basar, M. Wen, R. Mesleh, M. Di Renzo, Y. Xiao, and H. Haas, "Index modulation techniques for next-generation wireless networks," *IEEE Access*, vol. 5, pp. 16693–16746, 2017.

[11] T. Mao, Q. Wang, Z. Wang, and S. Chen, "Novel index modulation techniques: a survey," *IEEE Communications Surveys & Tutorials*, vol. 21, no. 1, pp. 315–348, 2019.

[12] P. Yang, M. Di Renzo, Y. Xiao, S. Li, and L. Hanzo, "Design guidelines for spatial modulation," *IEEE Communications Surveys & Tutorials*, vol. 17, no. 1, pp. 6–26, 2015.

[13] R. Mesleh, H. Haas, S. Sinanovic, C. W. Ahn, and S. Yun, "Spatial modulation," *IEEE Transactions on Vehicular Technology*, vol. 57, no. 4, pp. 2228–2241, 2008.

[14] M. Wen, B. Zheng, K. J. Kim et al., "A survey on spatial modulation in emerging wireless systems: research progresses and applications," *IEEE Journal on Selected Areas in Communications*, vol. 37, no. 9, pp. 1949–1972, 2019.

[15] J. Wang, S. Jia, and J. Song, "Generalised spatial modulation system with multiple active transmit antennas and low complexity detection scheme," *IEEE Transactions on Wireless Communications*, vol. 11, no. 4, pp. 1605–1615, 2012.

[16] H. Qing, H. Yu, Y. Liu, and M. Wen, "Enhanced spatial modulation with generalized antenna selection in MISO channels," *IET Communications*, vol. 15, no. 16, pp. 2046–2053, 2021.

[17] Q. Li, M. Wen, M. D. Renzo, H. V. Poor, S. Mumtaz, and F. Chen, "Dual-hop spatial modulation with a relay transmitting its own information," *IEEE Transactions on Wireless Communications*, vol. 19, no. 7, pp. 4449–4463, 2020.

[18] S. Lin, B. Zheng, F. Chen, F. Ji, and H. Yu, "Soft demodulators based on deterministic SMC for single-carrier GSM in broadband channels," *IEEE Journal on Selected Areas in Communications*, vol. 37, no. 9, pp. 1973–1985, 2019.

[19] B. Zheng, M. Wen, F. Chen, N. Huang, F. Ji, and H. Yu, "The k-best sphere decoding for soft detection of generalized spatial modulation," *IEEE Transactions on Communications*, vol. 65, no. 11, pp. 4803–4816, 2017.

[20] B. Farhang-Boroujeny and H. Moradi, "OFDM inspired waveforms for 5G," *IEEE Communications Surveys & Tutorials*, vol. 18, no. 4, pp. 2474–2492, 2016.

[21] B. Zheng and R. Zhang, "Intelligent reflecting surface-enhanced OFDM: channel estimation and reflection optimization," *IEEE Wireless Communications Letters*, vol. 9, no. 4, pp. 518–522, 2020.

[22] Y. Liu, F. Ji, M. Wen, D. Wan, and B. Zheng, "Vector OFDM with index modulation," *IEEE Access*, vol. 5, pp. 20135–20144, 2017.

[23] B. Zheng, C. You, and R. Zhang, "Intelligent reflecting surface assisted multi-user OFDMA: channel estimation and training design," *IEEE Transactions on Wireless Communications*, vol. 19, no. 12, pp. 8315–8329, 2020.

[24] E. Basar, U. Aygolu, E. Panayirci, and H. V. Poor, "Orthogonal frequency division multiplexing with index modulation," *IEEE Transactions on Signal Processing*, vol. 61, no. 22, pp. 5536–5549, 2013.

[25] M. Wen, B. Ye, E. Basar, Q. Li, and F. Ji, "Enhanced orthogonal frequency division multiplexing with index modulation," *IEEE Transactions on Wireless Communications*, vol. 16, no. 7, pp. 4786–4801, 2017.

[26] Q. Li, M. Wen, B. Clerckx, S. Mumtaz, A. Al-Dulaimi, and R. Q. Hu, "Subcarrier index modulation for future wireless networks: principles, applications, and challenges," *IEEE Wireless Communications*, vol. 27, no. 3, pp. 118–125, 2020.

[27] M. Wen, Q. Li, and X. Cheng, *Index Modulation for OFDM Communications Systems*, Springer International Publishing AG, Cham, Switzerland, 2021.

[28] N. Ishikawa, S. Sugiura, and L. Hanzo, "Subcarrier-index modulation aided OFDM - will it work?," *IEEE Access*, vol. 4, pp. 2580–2593, 2016.

[29] M. Wen, X. Cheng, M. Ma, B. Jiao, and H. V. Poor, "On the achievable rate of OFDM with index modulation," *IEEE Transactions on Signal Processing*, vol. 64, no. 8, pp. 1919–1932, 2016.

[30] M. Wen, X. Cheng, L. Yang, Y. Li, X. Cheng, and F. Ji, "Index modulated OFDM for underwater acoustic communications," *IEEE Communications Magazine*, vol. 54, no. 5, pp. 132–137, 2016.

[31] Y. Liu, F. Ji, H. Yu, F. Chen, D. Wan, and B. Zheng, "Enhanced coordinate interleaved OFDM with index modulation," *IEEE Access*, vol. 5, pp. 27504–27513, 2017.

[32] Q. Li, M. Wen, E. Basar, and F. Chen, "Index modulated OFDM spread spectrum," *IEEE Transactions on Wireless Communications*, vol. 17, no. 4, pp. 2360–2374, 2018.

[33] M. Wen, X. Chen, Q. Li, E. Basar, Y.-C. Wu, and W. Zhang, "Index modulation aided subcarrier mapping for dual-hop OFDM relaying," *IEEE Transactions on Communications*, vol. 67, no. 9, pp. 6012–6024, 2019.

[34] H. Qing, H. Yu, Y. Liu, W. Duan, M. Wen, and F. Ji, "Distributed cooperative OFDM-IM system," *China Communications*, vol. 17, no. 9, pp. 167–176, 2020.

[35] T. Mao, Z. Wang, Q. Wang, S. Chen, and L. Hanzo, "Dual-mode index modulation aided OFDM," *IEEE Access*, vol. 5, pp. 50–60, 2017.

[36] M. Wen, E. Basar, Q. Li, B. Zheng, and M. Zhang, "Multiple-mode orthogonal frequency division multiplexing with index modulation," *IEEE Transactions on Communications*, vol. 65, no. 9, pp. 3892–3906, 2017.

[37] Q. Li, M. Wen, E. Basar, H. V. Poor, B. Zheng, and F. Chen, "Diversity enhancing multiple-mode OFDM with index modulation," *IEEE Transactions on Communications*, vol. 66, no. 8, pp. 3653–3666, 2018.

[38] M. Wen, Q. Li, E. Basar, and W. Zhang, "Generalized multiple-mode OFDM with index modulation," *IEEE Transactions on Wireless Communications*, vol. 17, no. 10, pp. 6531–6543, 2018.

[39] J. Zheng and R. Chen, "Achieving transmit diversity in OFDM-IM by utilizing multiple signal constellations," *IEEE Access*, vol. 5, pp. 8978–8988, 2017.

[40] Z. Hu, J. Yang, P. Guo, and Q. Li, "Orthogonal frequency division multiplexing with cascade index modulation," *IET Communications*, vol. 16, no. 10, pp. 1057–1070, 2022.

[41] Z. Hu, F. Chen, Y. Liu, S. Liu, H. Yu, and F. Ji, "Low-complexity detection for multiple-mode OFDM with index modulation," *Physical Communication*, vol. 34, pp. 38–47, 2019.

[42] B. Zheng, F. Chen, M. Wen, F. Ji, H. Yu, and Y. Liu, "Low-complexity ML detector and performance analysis for OFDM with in-phase/quadrature index modulation," *IEEE Communications Letters*, vol. 19, no. 11, pp. 1893–1896, 2015.

[43] J. Hoydis, S. ten Brink, and M. Debbah, "Massive MIMO in the UL/DL of cellular networks: how many antennas do we need?," *IEEE Journal on Selected Areas in Communications*, vol. 31, no. 2, pp. 160–171, 2013.

[44] E. Basar, "Multiple-input multiple-output OFDM with index modulation," *IEEE Signal Processing Letters*, vol. 22, no. 12, pp. 2259–2263, 2015.

[45] T. Datta, H. S. Eshwaraiah, and A. Chockalingam, "Generalized space-and-frequency index modulation," *IEEE Transactions on Vehicular Technology*, vol. 65, no. 7, pp. 4911–4924, 2016.

[46] E. Basar, "On multiple-input multiple-output OFDM with index modulation for next generation wireless networks," *IEEE Transactions on Signal Processing*, vol. 64, no. 15, pp. 3868–3878, 2016.

[47] Z. Hu, S. Lin, B. Zheng, F. Chen, Q. Wang, and Y. Wei, "Low complexity subcarrier-wise detection for MIMO-OFDM with index modulation," *IEEE Access*, vol. 5, pp. 23822–23832, 2017.

[48] B. Zheng, M. Wen, E. Basar, and F. Chen, "Multiple-input multiple-output OFDM with index modulation: low-complexity detector design," *IEEE Transactions on Signal Processing*, vol. 65, no. 11, pp. 2758–2772, 2017.